

Flow field characteristics and separation performance of prismatic hydrocyclone

Yuekan Zhang ¹, Qingyun Zhang ², Wei Hu ³, Shuo Han ⁴

¹ College of Mechanical & Electronic Engineering, Shandong University of Science and Technology, Qingdao 266590, China

Corresponding author: zhangyk2007@sdust.edu.cn (Yuekan Zhang)

Abstract: Separation of organic matter and grit in sludge is essential for effective sludge recycling. However, the high viscosity and fine particles of sludge cause organic matter to adhere to grit surfaces, making separation challenging. To address this issue, we propose a novel prismatic hydrocyclone that generates intense turbulent flows, under strong turbulence, the prism boundary layer's "elutriation" enhances particle separation, increasing particle looseness and improving grit removal efficiency in sludge. This study compares the separation performance of the prismatic hydrocyclone with that of a conventional hydrocyclone using numerical simulations. We also investigate how the number of prism edges affects flow field characteristics and separation performance. The results show that, unlike conventional hydrocyclone, prismatic hydrocyclones generally maintain lower static pressure, pressure drop, and the diameter of the air core, indicating lower energy consumption and higher processing capacity. When the number of edges is 6, the pressure drop is the most reduced compared to the conventional hydrocyclone, which is 22.17%. Under similar feed velocity, the centrifugal intensity in prismatic hydrocyclones is reduced compared to conventional hydrocyclone, lower centrifugal forces mitigate the risk of fine particles moving toward the wall under high-speed conditions. Meanwhile, turbulence intensity beneath the vortex finder decreases, which signifies the flow field is more stable, and grit removal efficiency in sludge is improved.

Keywords: prismatic hydrocyclone, flow field characteristics, separation performance, turbulence

1. Introduction

Municipal sludge contains significant organic matter and grit, which have substantial utilization value. Efficient separation of organic matter and grit from sludge is a prerequisite for sludge utilization. Hydrocyclones, with their simple structure, small footprint, and high separation efficiency, play an irreplaceable role in particle separation (Almilly and Chasib, 2023; Wang et al., 2024; Bai et al., 2021; Ji et al., 2023). However, due to the high viscosity of sludge, organic matter tends to adhere to grit surfaces, making separation challenging (Cao et al., 2021). Therefore, developing hydrocyclone-based fine particle separation technology is crucial to overcoming bottlenecks in fine particle separation and promoting sludge resource recycling and harmonious environmental development.

Sholl et al. demonstrated that physical separation is a resource separation method with low energy consumption, low emissions, and low pollution. Cyclonic separation, a typical physical separation method, effectively separates insoluble particles based on centrifugal sedimentation (Sholl et al., 2016). Due to its excellent performance, it is widely used in liquid-solid separation, classification, and purification in metallurgy, coal, petroleum, chemical, energy, and environmental protection industries, and is considered one of the "cleanest" separation methods (Silva et al., 2020; Khatri et al., 2020; Thiemsakul et al., 2024; Izquierdo et al., 2024). Successful particle separation in a hydrocyclone requires not only a necessary particle size or density difference between the solid and liquid phases but also a stable flow field inside the hydrocyclone. Severe turbulent fluctuations and disturbances can disrupt the flow field stability. When turbulent kinetic energy exceeds centrifugal separation energy, particles of different sizes mix, making separation difficult and significantly reducing the separation efficiency

of fine particles. Thus, high turbulence intensity or turbulent kinetic energy is a technical bottleneck for efficient fine particle separation, as it hinders the smooth progress of cyclonic separation.

To regulate the influence of the flow field on particle separation, many scholars have conducted in-depth research on fine particle classification, examining structural parameters, operational parameters, turbulent flow, and particle phase interactions. Some have strengthened centrifugal intensity by increasing the feed pressure of the hydrocyclone (Izquierdo et al., 2023; Jiang et al., 2021), while others have offset particle migration resistance by raising the feed temperature (Hamza et al., 2019; Salmanizade et al., 2021). Structural modifications, such as introducing a symmetrical structure in the inlet (Liang et al., 2024; Zhao et al., 2021; Li et al., 2021) or changing the inlet structure (Noroozi and Hashemabadi, 2011; Razmi et al., 2019; Ye et al., 2019), have been employed to reduce flow field disturbances caused by abrupt changes in particle Reynolds number. Mini-hydrocyclones (Liu et al., 2023; Vega-Garcia et al., 2020; Abdollahzadeh et al., 2022) have been used to enhance the centrifugal separation process, and alter the length of the vortex finder (Hsu and Wu, 2010; Li et al., 2021; Zhang et al., 2021) or the column structure (Ni et al., 2019; Hou et al., 2023) has been shown to improve separation accuracy. Additionally, electric and magnetic fields (Lavrinenko and Sysa, 2023; Zhou et al., 2023; Peng et al., 2024; Gong et al., 2023) have been introduced to regulate turbulent flow inside the hydrocyclone. These methods can suppress turbulent fluctuations and improve the overall classification efficiency of the hydrocyclone.

However, studies have also found significant Reynolds shear stress and turbulent kinetic energy near the hydrocyclone wall. High turbulent kinetic energy can enhance the "elutriation" of particles within the wall boundary layer, causing some misplaced fine particles to return to the main separation zone for re-separation, which benefits particle movement and separation accuracy. Thus, turbulence has a dual effect on fine particle separation: it can cause disordered arrangement and random movement of particles, but it can also elutriate fine particles from the wall boundary layer, reducing particle misplacement and mixing.

In summary, although many improved fine particle separation measures have been proposed to address classification challenges by regulating the flow field, the research on the effects of turbulence on particle motion and separation is still insufficient to comprehensively reveal the fine particle separation mechanism inside the hydrocyclone. Herein, we propose a prismatic hydrocyclone to enhance particle looseness in the outer swirling flow. When the outer swirling flow passes through the corners, its motion state changes, forming local turbulence. The prism increases turbulence intensity near the hydrocyclone wall, allowing highly viscous, fine sludge particles that mistakenly enter the boundary wall to be elutriated and returned to the separation zone, thereby improving grit removal efficiency in sludge. In this study, we compared and analyzed the flow field characteristics and separation performances of the proposed prismatic hydrocyclone and the conventional hydrocyclone using numerical simulations, and investigated the effects of the number of prism edges on flow field characteristics and separation performance.

2. Research method

2.1. Mechanism of proposed prismatic hydrocyclone for enhancing particle separation

Fig. 1 and Fig. 2 show the particle motion and particle stress inside the hydrocyclone. In the radial direction, solid particles are subject to the centripetal buoyancy F_{cenbuo} , centrifugal force F_{cenf} , and fluid drag force F_{hd} . Spherical solid particles are subject to the combined force of F_{cenf} and F_{cenbuo} as follows:

$$F_{cenf} + F_{cenbuo} = \frac{\pi d^3}{6r} (\rho_s - \rho) u_t^2 \quad (1)$$

where d is the size of spherical solid particles, ρ_s is the particle density, ρ is the density of liquid phases, and u_t is the tangential velocity of the particles.

In the radial direction, particles are subject to the drag force of fluid F_{hd} as follows:

$$F_{hd} = -\xi A \frac{\rho u^2}{2} = -\frac{\xi \rho \pi d^2 u^2}{8} \quad (2)$$

where ξ refers to the resistance coefficient, A refers to the projected area of the spherical solid particles ($A = \pi d^2/4$), and u refers to the relative velocity between the particles and the fluids in the radial direction.

According to Eq. (1) and Eq. (2), the resultant force of solid particles in the radial direction is:

$$F_r = \frac{\pi d^3}{6r} (\rho_s - \rho) u_t^2 - \frac{\xi \rho \pi d^2 u^2}{8} \quad (3)$$

When the relative velocity between the fluid and the solid particles reaches the centrifugal settling velocity u_{or} , the forces F_{centf} , F_{centf} , and F_{hd} reach equilibrium ($F_r=0$), and then:

$$U_{or} = \sqrt{\frac{4d(\rho_s-\rho)u_t^2}{3\xi\rho r}} \quad (4)$$

According to Eq. (4), the distribution of solid particles in the radial direction can be determined by:

$$d = \frac{3}{4} \frac{\xi \rho}{(\rho_s - \rho)} \left(\frac{U_{or}}{u_t} \right)^2 r \quad (5)$$

According to Eq. (5), the particle size is proportional to its rotational radius, so the particle size gradually increases from the axis to the wall. When a prismatic column segment is used, solid particles moving toward the corners experience an increase in rotational radius r , causing more coarse particles to migrate toward the corners. As these solid particles are spun out of the corners with the fluids, the rotational radius r decreases, leading to collisions with particles at the corners and generating a counter-

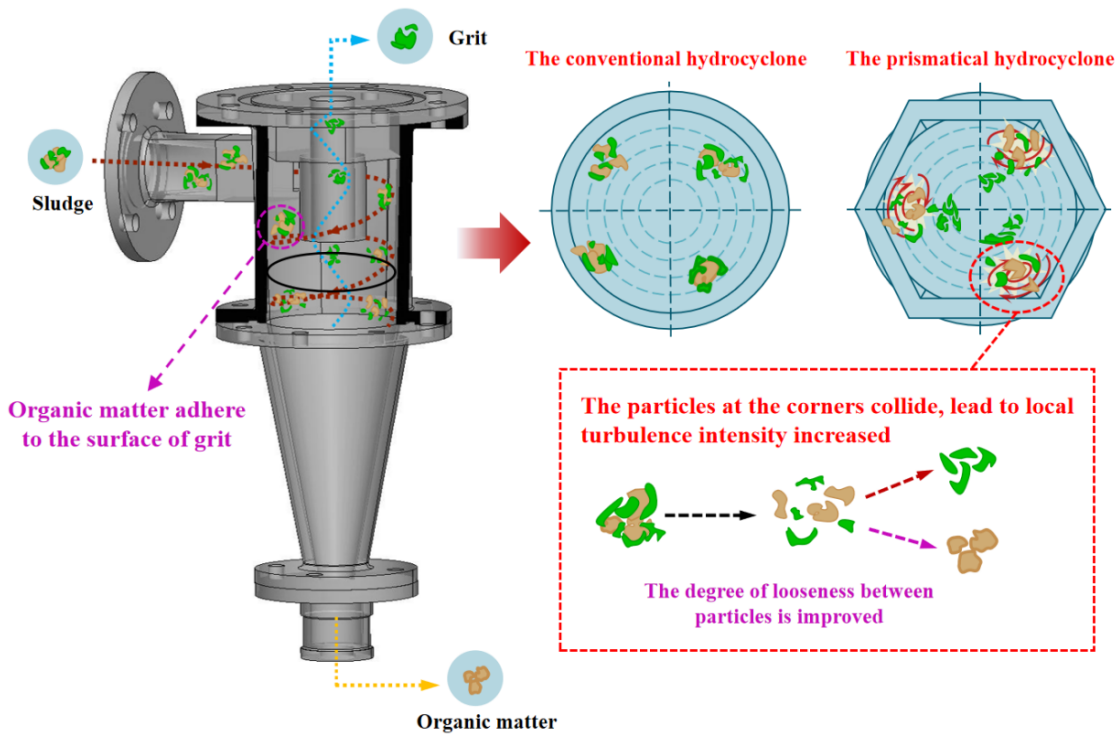


Fig. 1. Schematic of particle motion in hydrocyclone

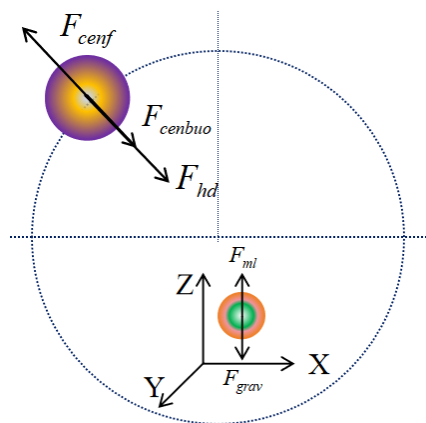


Fig. 2. Particle stress analysis diagram

force. This enhances local turbulence intensity, increases particle looseness, and creates an elutriation effect on the organic matter adhering to the grit surface, causing it to re-enter the separation zone and thereby improving the recovery rate of organic matter in the sludge. Additionally, the edges of the prismatic hydrocyclone disrupt the boundary layer of fluid flow in the column segment, reducing the boundary layer thickness, lowering resistance in the column segment, and ultimately decreasing energy consumption.

2.2. Mathematic model

Zhang et al. used the RSM model coupled with the VOF model and the Mixture model to investigate the effect of the inlet curvature radius on the separation performance of a hydrocyclone. He validated the model's accuracy by comparing the predicted results with experimental results obtained by other researchers (Zhang et al., 2017). Dos Anjos et al. compared the effects of turbulence models on the unsteady numerical simulation of liquid-liquid two-phase flow in a $\Phi 40$ mm hydrocyclone and concluded that the RSM model is the only turbulence model that can correctly reflect the tangential velocity distribution of the hydrocyclone (Anjos et al., 2021). Therefore, this study uses the RSM model to calculate turbulence, the VOF model to capture the gas-liquid interface, and the Mixture model to simulate particle-mixed phases.

The RSM model removes the assumption of isotropic turbulent viscosity and comprehensively considers the anisotropy of turbulent flow. With the highest accuracy in predicting complex flow fields, this model is suitable for the numerical simulation of the flow field inside a hydrocyclone. Its transport equation is shown in Eq. (6):

$$\frac{\partial(\overline{\rho u_i' u_j'})}{\partial t} + \frac{\partial(\overline{\rho u_k u_i' u_j'})}{\partial x_k} = D_{T,ij} + D_{L,ij} + P_{ij} + G_{ij} + \Phi_{ij} + \varepsilon_{ij} + F_{ij} \quad (6)$$

where $\overline{\rho u_i' u_j'}$ is the mean Reynolds stress, $D_{T,ij}$ is the turbulent diffusion term, $D_{L,ij}$ is the molecular viscosity diffusion term, P_{ij} is the stress generation term, G_{ij} is the buoyancy generation term, Φ_{ij} is the pressure strain term, ε_{ij} is the viscous dissipation term, and F_{ij} is the fluid rotation generation term.

The VOF model is generally used for tracking two or more immiscible fluids. By solving the momentum equations and processing the volume fractions of different fluids within the computational domain, the gas-liquid two-phase flow inside the hydrocyclone can be simulated, thus capturing the air core. In the VOF model, the sum of the volume fractions of all phases within each unit equals 1, as shown below:

$$\sum_{q=1}^n \alpha_q = 1 \quad (7)$$

where α_q is the volume fraction of the qth phase per unit.

The Mixture model is suitable for simulating two-phase or multi-phase mixed fluids. By solving the continuity equation and the momentum equation of the mixed fluid, the separation performance of the fluid inside the hydrocyclone can be calculated. The continuity equation of the Mixture model is:

$$\frac{\partial}{\partial t} (\rho_m) + \nabla \cdot (\rho_m \vec{v}_m) = \dot{m} \quad (8)$$

where ρ_m refers to the density of the mixture, \dot{m} refers to the mass transfer, and \vec{v}_m refers to the mean mass velocity of the mixture.

The momentum equation of the Mixture model is:

$$\frac{\partial}{\partial t} (\rho_m \vec{v}_m) + \nabla \cdot (\rho_m \vec{v}_m \vec{v}_m) = -\nabla \cdot \vec{P} + \nabla \cdot [\mu_m (\nabla \cdot \vec{v}_m + \nabla \cdot \vec{v}_m^T)] + \rho_m \vec{g} + \vec{F} + \nabla \cdot (\sum_{k=1}^n \alpha_k \rho_k \vec{v}_k^r \vec{v}_k^r) \quad (9)$$

where n refers to the total number of phases, μ_m refers to the viscosity of the mixed phase, ρ_k refers to the kth phase density and \vec{v}_k^r refers to is the relative slip velocity of the kth phase with respect to the mixed phase.

2.3. Numerical Simulation

SolidWorks 2022 was used for modeling. Fig. 3 illustrates the structure of the hydrocyclone, while Table 1 lists its key structural parameters. ICEM 17.0 was employed for hexahedral meshing of a conventional hydrocyclone, and prismatic hydrocyclones, as depicted in Fig. 4. The number of grids is 130720, 147152, 136556, and 124292 respectively, and the mesh quality is above 0.5 as shown in Fig. 5, meeting the requirement of calculation accuracy. The origin of the coordinate system was set at the center of the

hydrocyclone vortex finder top, with the positive Z-axis directed downward. For numerical simulation, hydrocyclone sections $Z_1 = 115 \text{ mm}$, $Z_2 = 200 \text{ mm}$, and $Y = 0 \text{ mm}$ were selected as references.

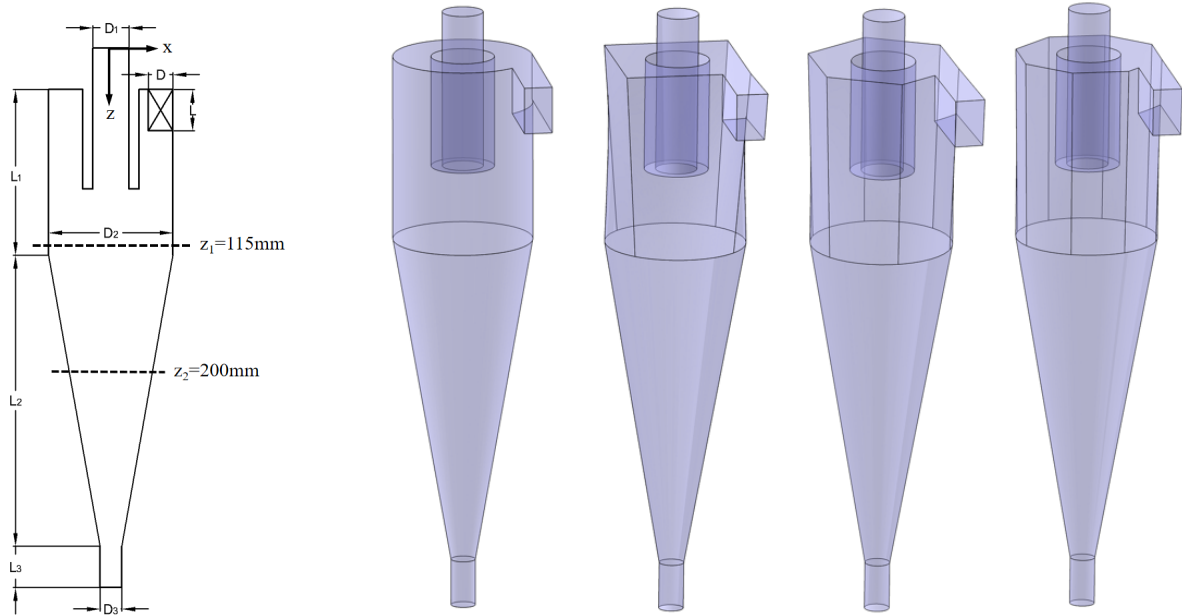


Fig. 3. Structure of the hydrocyclone

Table 1. Key structural parameters of the hydrocyclone

Structural parameter	Value/mm
Diameter of the vortex finder (D_1)	22
Diameter of the hydrocyclone (D_2)	75
Diameter of the apex (D_3)	13
Length of cylindrical section (L_1)	100
Length of conical section (L_2)	175.81
Length of apex (L_3)	25
Inlet ($L \times D$)	25×15
Length of vortex finder	60

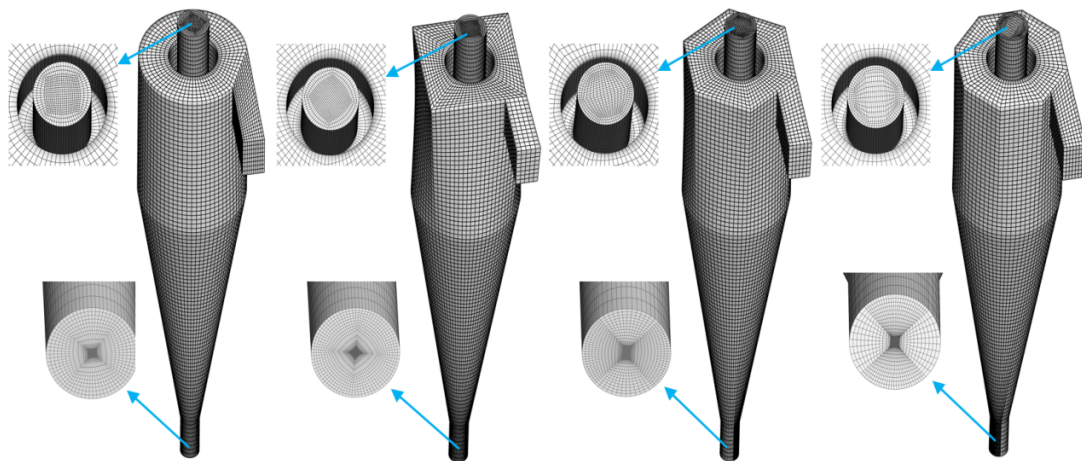


Fig. 4. Meshing of hydrocyclone

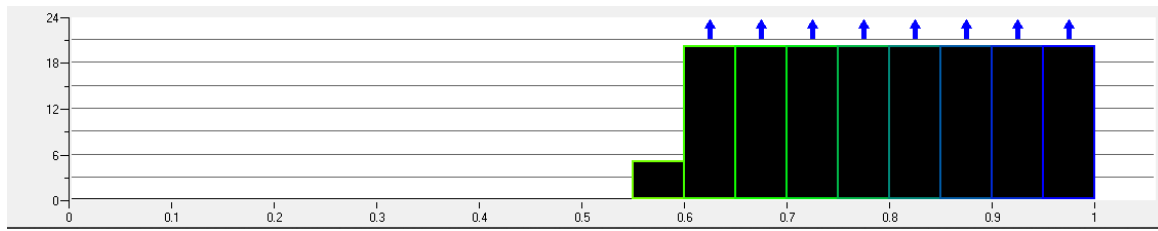


Fig. 5. Mesh quality

Numerical simulations were conducted using Fluent 2022R2. Turbulence calculations employed the RSM model, while the VOF model was utilized to simulate the gas-liquid interface. The primary phase consisted of water, with air as the secondary phase. The air phase backflow volume fraction was set to 1, indicating the hydrocyclone was initially filled with air, and the initial air volume fraction was also set to 1.

The Mixture model was employed to simulate the distribution of sludge particles within the hydrocyclone. Under engineering practice data, the density of inorganic sludge particles was set to 2650 kg/m^3 , with a mass concentration of 70%. The particle size and volume fraction distributions are detailed in Table 2. Organic sludge particles were assigned a density of 910 kg/m^3 , with a mass concentration of 30%. Two particle sizes, $40 \mu\text{m}$, and $100 \mu\text{m}$, were used in the simulation, with corresponding contents of 58.2% and 41.8%, and volume fractions of 0.765% and 0.549%, respectively.

The simulation employed a transient method. Inlet conditions were set as "Velocity-inlet" at 4.5 m/s , while all outlets were defined as "Pressure-outlet". Pressure-velocity coupling used the "SIMPLE" method, with pressure spatial discretization set to "PRESTO" and other discretization methods set to "QUICK". Convergence was determined based on the balance of phase flow rates at the inlet and outlet conditions.

Table 2. Particle size distribution of grit

Size/ μm	Particle content/%	Volume fraction/%
5	13.56	0.145
15	15.32	0.164
25	16.26	0.174
35	15.13	0.162
45	14.20	0.152
65	13.41	0.143
95	12.12	0.130
Total	100	1.070

2.4. Model validation

To validate the accuracy of the mathematical model, numerical simulation data were compared with experimental results from Hsieh and Rajamani (Hsieh and Rajamani, 1988). As depicted in Fig. 6 (a), (b), and (c), the simulation results closely align with the experimental findings. This consistency indicates that the chosen turbulence model, multi-phase flow model, and calculation methodology are reliable.

3. Simulation results and analysis

3.1. Pressure distribution

The pressure field within a hydrocyclone reflects its processing capacity and energy consumption, making exploration of this field highly significant. Fig. 7 compares the static pressure curves of prismatic hydrocyclones with those of a conventional hydrocyclone in section Z1. Both configurations exhibit similar axially symmetrical pressure distribution patterns, with pressure peaking at the wall, decreasing towards the axis center, and reaching negative values at the center. However, the prismatic hydrocyclones generally maintain lower pressures compared to the conventional hydrocyclone. This difference arises because fluid flow through the edges of prismatic hydrocyclones alters direction,

creating multiple micro eddy currents at the corners that promote turbulence near the wall. This turbulence reduces the likelihood of flow separation in the turbulent boundary layer, thereby lowering fluid resistance and pressure.

Fig. 8 compares the pressure drops at section Z_1 between prismatic hydrocyclones and conventional hydrocyclone. When the prismatic hydrocyclones feature 4, 6, and 8 edges, the pressure drops are

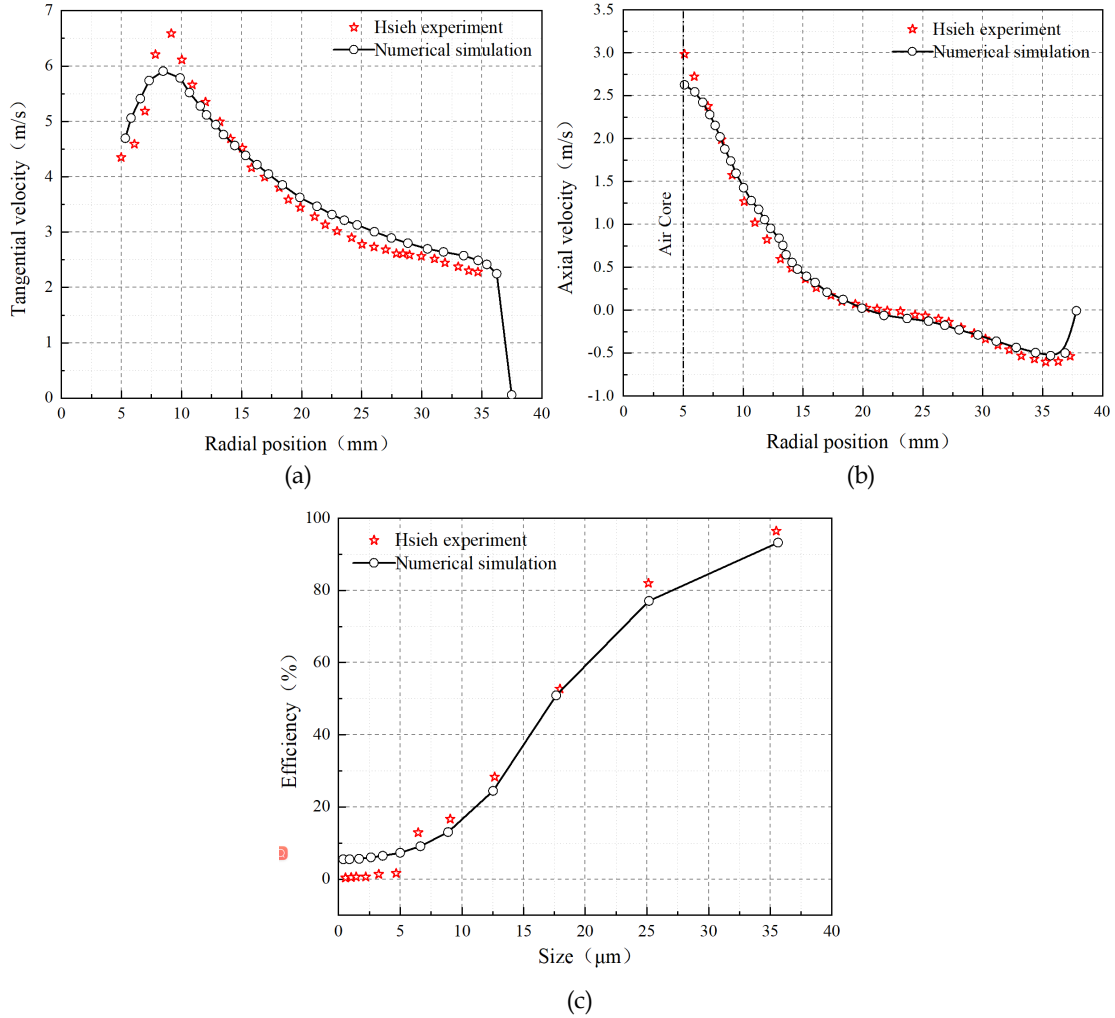


Fig. 6. Comparison of simulation and experimental results

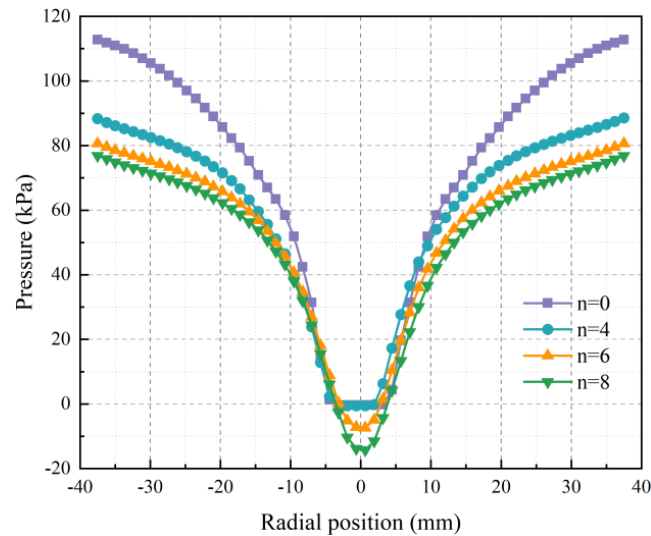


Fig. 7. Pressure at Z_1 section

reduced by 21.45%, 22.17%, and 18.80%, respectively, compared to the conventional hydrocyclone ($n=0$). Notably, the six-edged prismatic hydrocyclone exhibits the smallest pressure drop, indicating lower energy consumption and higher processing capacity compared to other configurations.

Fig. 9 illustrates pressure contours across various sections of prismatic hydrocyclones and a conventional hydrocyclone. Compared to conventional hydrocyclone, prismatic hydrocyclones exhibit lower static pressure at sections of similar heights, with pressures decreasing as the number of edges increases. This reduction in pressure is attributed to the altered flow field dynamics and decreased boundary layer thickness resulting from the improved column segment structure. Lower pressure levels also contribute to reduced wear on the hydrocyclone walls. Therefore, transforming the column segment of a hydrocyclone into a prismatic shape offers potential benefits such as lower energy consumption and extended service life of the hydrocyclone.

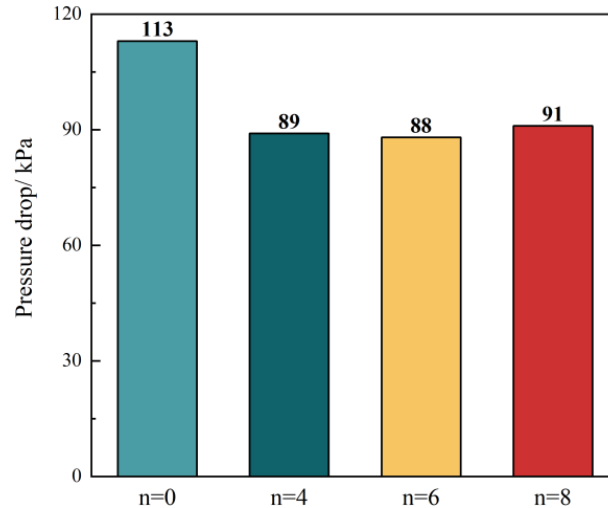


Fig. 8. Pressure drop

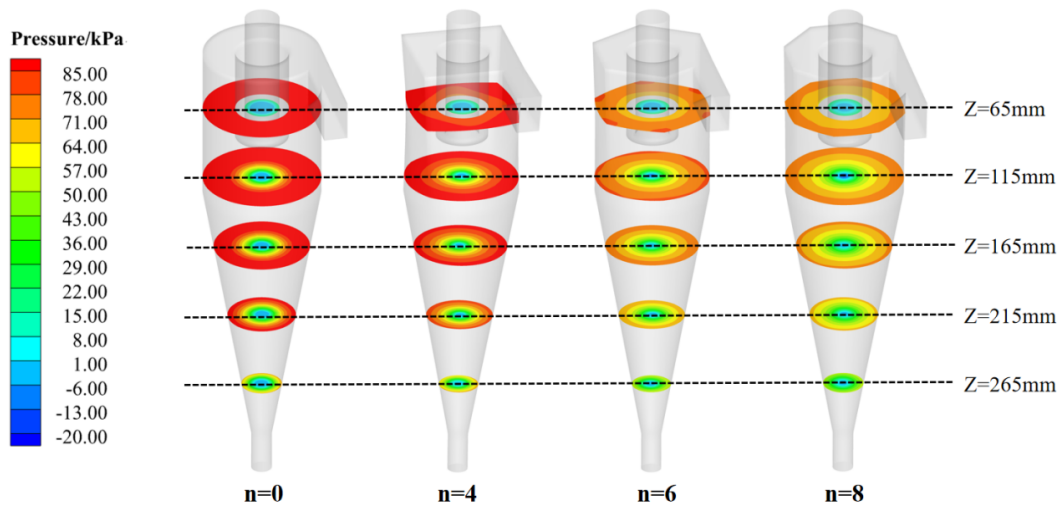


Fig. 9. Contours of pressures on different sections of prismatic hydrocyclones and the conventional hydrocyclone

3.2. Tangential velocity distribution

Fig. 10 presents the tangential velocity distribution curves at sections Z1 and Z2 for prismatic hydrocyclones and conventional hydrocyclone. The tangential velocity distribution patterns within both types of hydrocyclones generally exhibit an "M"-shaped profile with good axial symmetry. Specifically, velocity increases from the hydrocyclone wall towards the axis, reaching a peak at the boundary between the forced vortex and the free vortex.

Fluids enter the hydrocyclone tangentially from the wall, transitioning from linear to rotational motion due to the hydrocyclone's unique geometric structure and high-pressure feed method. This

setup induces complex turbulent flows, particularly near the wall and at the turning points of the outer and inner swirling flows. Turbulence disrupts the stability of the flow field and the orderly arrangement of fine particles by size, leading to random particle motion and decreased efficiency in fine particle separation.

In this study, conventional cylindrical hydrocyclones were transformed into a prismatic structure. As depicted in Fig. 10, the maximum tangential velocity observed in prismatic hydrocyclones was lower than that in conventional hydrocyclones. This suggests that the centrifugal intensity in prismatic hydrocyclones is reduced compared to cylindrical ones under similar feed pressures. Lower centrifugal forces mitigate the risk of fine particles moving towards the wall under high-speed conditions, thus preventing their mixing into the outer swirling flow and reducing the likelihood of organic matter adhering to the sludge wall.

Furthermore, reduced tangential velocity helps minimize inner wall friction, thereby lowering hydrocyclone wear. Additionally, smoother variations in tangential velocity within prismatic hydrocyclones facilitate the formation of a stable separation density layer, potentially improving overall hydrocyclone separation performance.

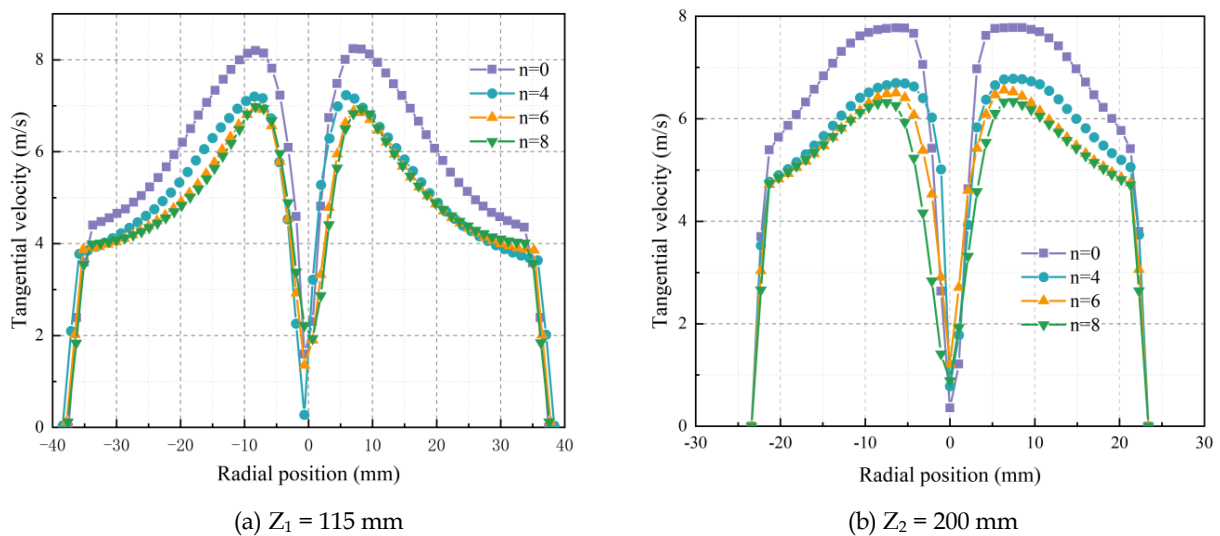


Fig. 10. Tangential velocity distribution curves

3.3. Axial velocity distribution

Fig. 11 displays the axial velocity distribution curves at sections $Z_1 = 115$ mm and $Z_2 = 200$ mm for prismatic hydrocyclones and conventional hydrocyclone. Both types of hydrocyclones exhibit axially symmetric distribution of axial velocities. Axial velocity directly influences the residence time of material within the hydrocyclone. At sections Z_1 and Z_2 , the axial velocity at the wall of prismatic hydrocyclones is slightly lower than that of the conventional hydrocyclone. This difference extends the residence time of the outer swirling flow inside the hydrocyclone, facilitating more thorough particle separation. Near the central axis of the hydrocyclone, the axial velocity of prismatic hydrocyclones is lower compared to conventional hydrocyclones, indicating that transforming the column segment of the hydrocyclone into a prismatic shape stabilizes the flow field and enhances separation performance.

The locus of zero vertical velocity (LZVV) is formed by connecting points of zero axial velocity in each section of the hydrocyclone, as depicted in Fig. 12. Within LZVV, fluid flows upward to form the inner swirling flow, which exits through the vortex finder. Outside LZVV, fluid flows downward to form the outer swirling flow, which exits through the apex.

Fig. 12 illustrates the distribution map of LZVV, showing persistent turbulent fluctuations inside the hydrocyclone that increase with the number of edges. Optimizing a conventional cylindrical hydrocyclone to a prismatic structure allows for the use of wall turbulence elutriation techniques, enhancing turbulent diffusion at the hydrocyclone boundary layer and loosening particles. This process facilitates the removal of fine particles mixed with coarse ones, thereby improving the separation accuracy of the hydrocyclone.

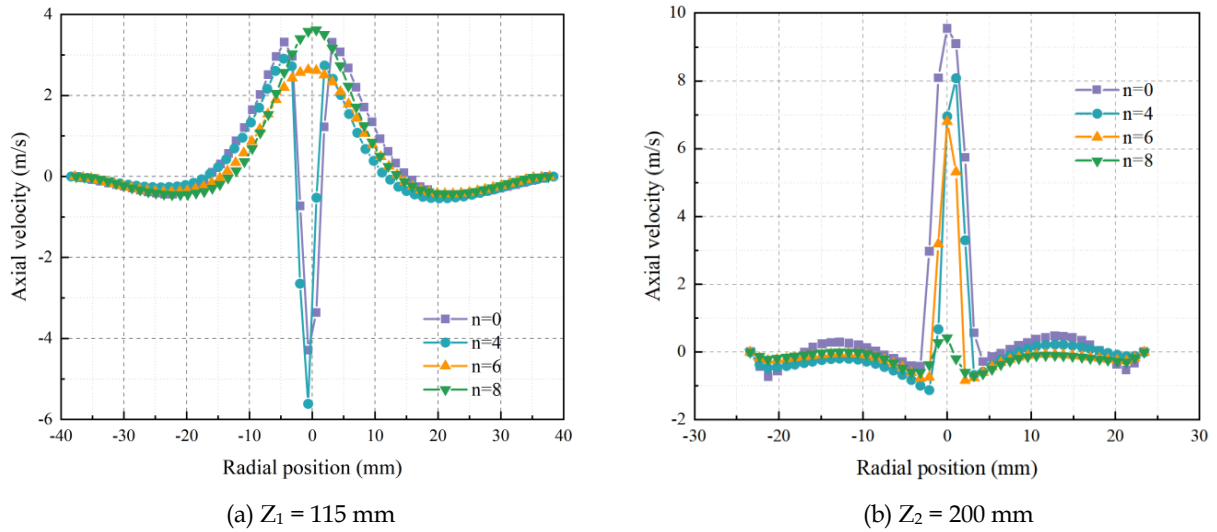


Fig. 11. Axial velocity distribution curves

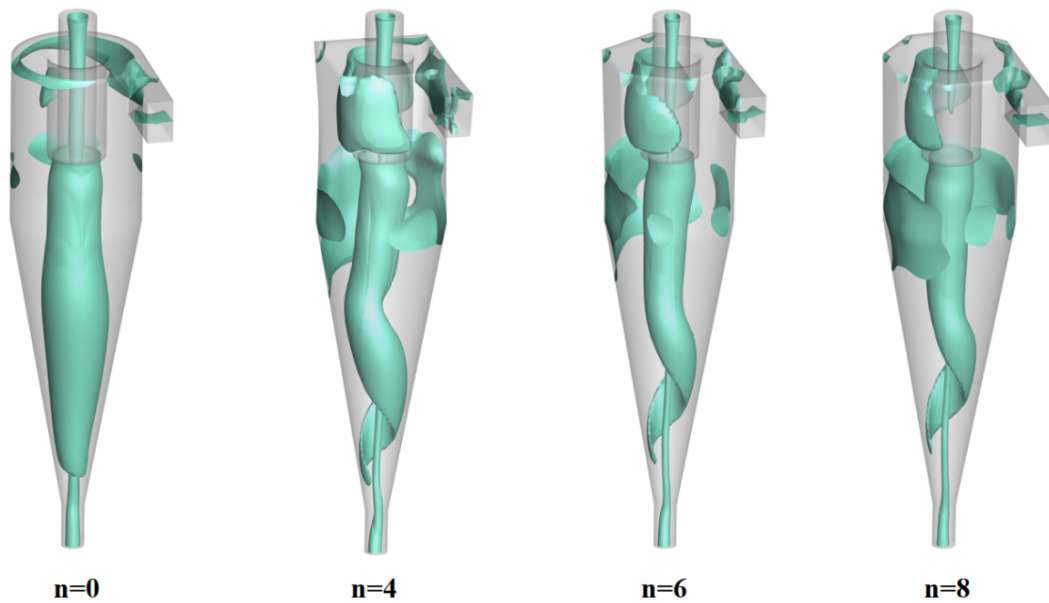


Fig. 12. LZVV

3.4. Air core

The formation of an air core is a crucial indicator of stable flow within a hydrocyclone, significantly influencing static pressure distribution, velocity patterns, and turbulence intensity in the flow field. Fig. 13 illustrates the formation and evolution of the air core in prismatic hydrocyclones and conventional hydrocyclone. In the Fig., the red color represents the air phase, while the blue color represents the water phase. Initially, the hydrocyclone was filled with air. Over time, the proportion of the air phase gradually decreased while the water phase increased, leading to the formation of an unstable, fluctuating air core. As the separation process continued, a stable air core eventually developed.

Both prismatic hydrocyclones and conventional hydrocyclone reached a stable flow state around 0.5 seconds, as shown in Fig. 13. Subsequently, the diameter of the air core in prismatic hydrocyclones gradually reduced, and in the case of the octagonal prismatic hydrocyclone, the air core eventually disappeared. This observation indicates that prismatic hydrocyclones have a smaller air core area, allowing a larger internal flow field area to participate in separation. Consequently, under identical operational conditions, prismatic hydrocyclones can effectively enhance the processing capacity of the hydrocyclone.

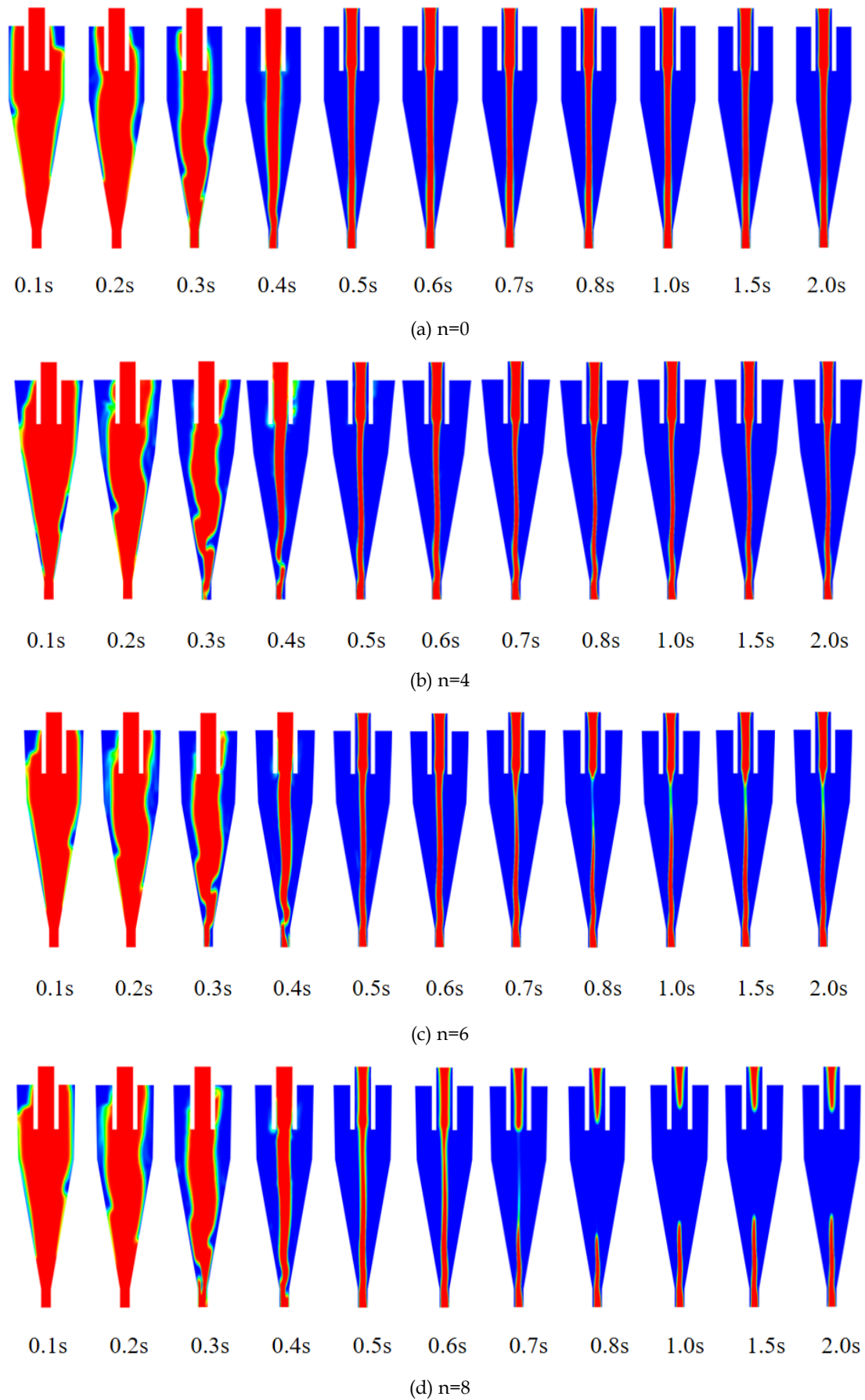


Fig. 13. Air core formation process

3.5. Turbulent intensity

Turbulent kinetic energy significantly influences both the separation efficiency and energy consumption of hydrocyclones. Fig. 14 illustrates the turbulence intensity contours in prismatic hydrocyclones and a conventional hydrocyclone. Compared to the conventional design, prismatic hydrocyclones exhibit higher turbulence intensity near the wall. This enhancement is attributed to particle collisions occurring as fluids pass through the corners, which disrupts the ordered distribution of particles within the hydrocyclone and increases particle looseness. Consequently, organic matter adhering to grit is elutriated and reintroduced into the separation zone, thereby enhancing sludge recovery rates.

In contrast, the conventional hydrocyclone shows increased turbulent intensity near the vortex finder and beneath the air core, leading to substantial energy losses and coarse particle overflow. Upon optimization to a prismatic structure, turbulence intensity in these areas notably decreases. This reduction signifies that prismatic hydrocyclones effectively mitigate energy losses, stabilize the flow field beneath the vortex finder, and reduce the likelihood of organic matter from sludge re-entering the outer swirling flow. As a result, prismatic hydrocyclones contribute to improved sludge separation accuracy.

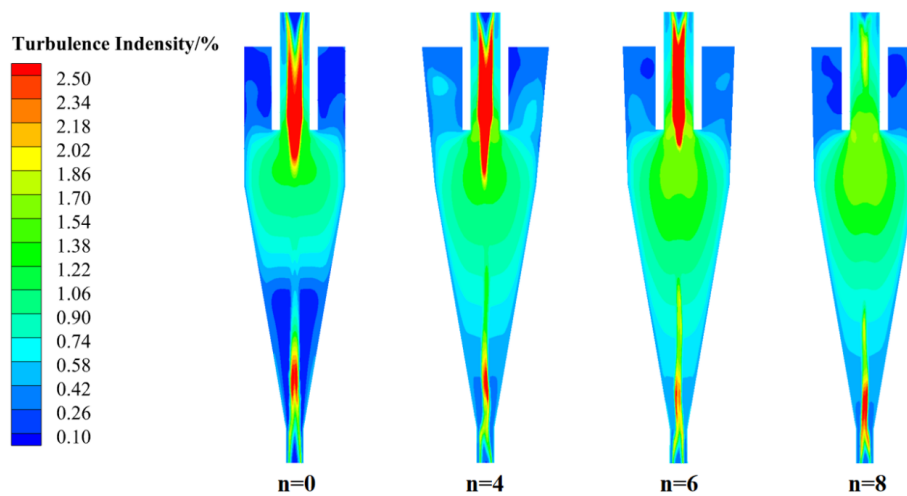


Fig. 14. Contours of turbulent intensity at the $Y = 0$ mm plane

3.6. Separation of organic matter and grit in sludge

Fig. 15 depicts the trajectory of particles in a prismatic hydrocyclone under turbulent conditions. As observed, as particles radially settle in the hydrocyclone, the centrifugal force gradually diminishes. Particle interactions primarily involve mechanical collisions during radial settling, influencing particle trajectories and distribution within the hydrocyclone. These collisions delay particle settling, significantly restricting the efficiency and effectiveness of fine particle separation.

Mechanical collisions between particles exert forces on the particle flow. When large particles collide with small particles, the momentum transfer from large to small particles reduces the velocity disparity between them but disrupts the ordered radial distribution of particles by size. Such collisions occurring on the locus of zero vertical velocity (LZVV) can greatly reduce separation accuracy.

When large particles settling outward collide with fine particles moving inward, the large particles experience minimal impact while the fine particles, due to their greater fluid followability, quickly resume their motion. However, if fine particles adhere to large particles during collisions, the material intended for overflow may erroneously enter the boundary layer, diminishing separation accuracy. In such cases, the turbulent elutriation effect within the boundary layer generated by prisms can help fine particles misplaced near the wall return to the main separation zone, thereby improving separation accuracy.

Fig. 16 (a) presents the concentration contours of $40 \mu\text{m}$ organic particles in prismatic hydrocyclones and a conventional hydrocyclone. Compared to the conventional design, prismatic hydrocyclones show significantly reduced organic particle concentration in the conical section, concentrating organic matter in the column segment. This configuration allows more organic matter from the sludge to enter the

inner swirling flow and discharge through the overflow, thereby enhancing organic matter recovery in the sludge.

Fig. 16 (b) displays the distribution of 100- μ m organic particles in prismatic hydrocyclones and conventional hydrocyclone. Here too, prismatic hydrocyclones effectively reduce the content of large-sized organic particles at the bottom. Overall, the comparison shows that prismatic hydrocyclones with six prism edges exhibit optimal separation performance for both sizes of organic matter particles.

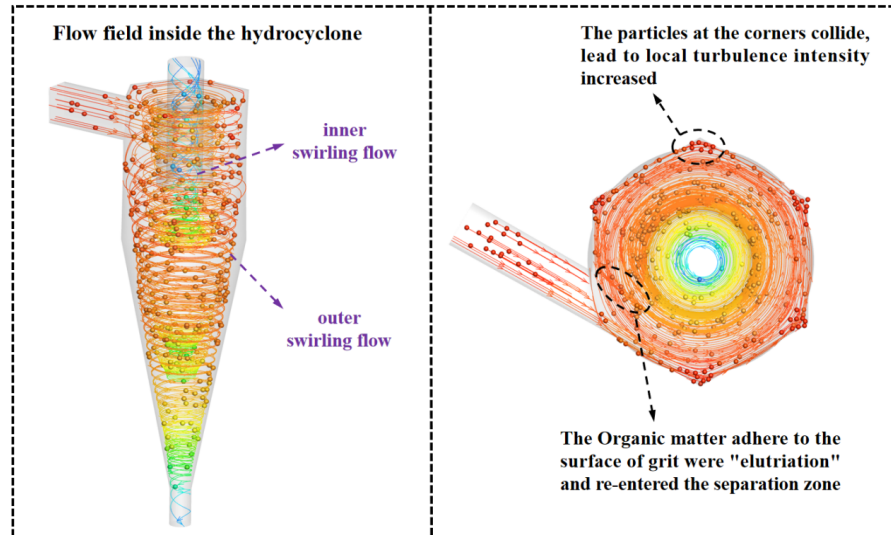


Fig. 15. The trajectory of particles in the prismatic hydrocyclone under turbulence

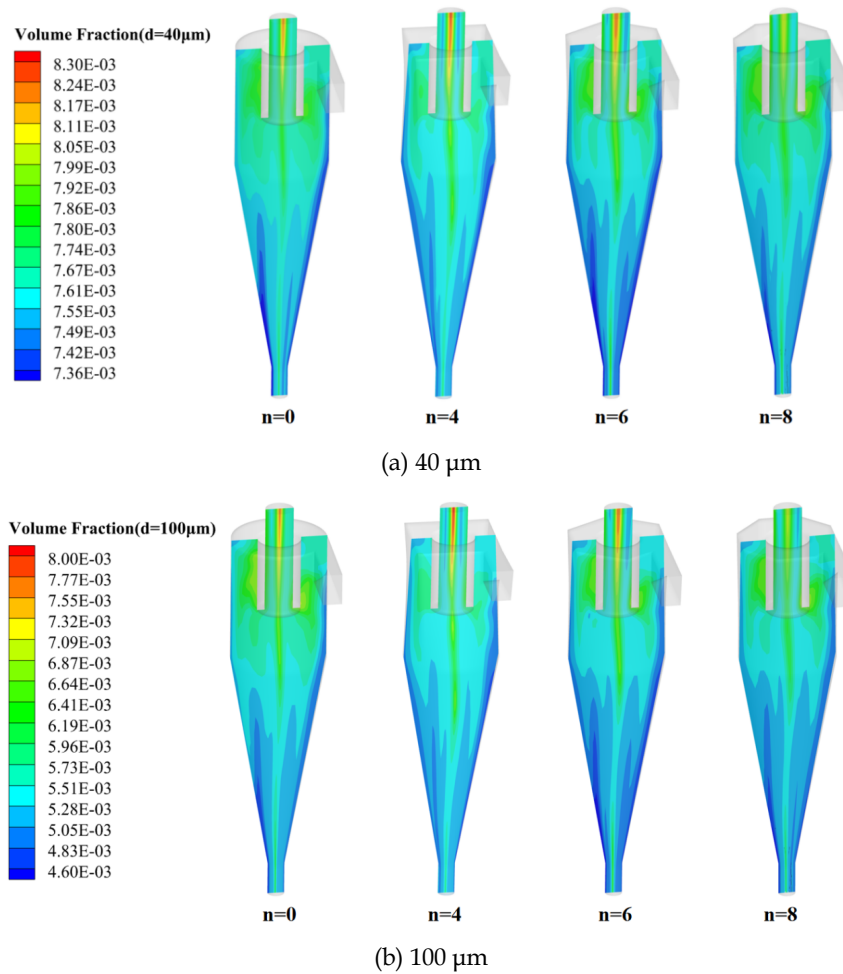


Fig. 16. Contours of organic particles at the Y = 0 mm plane

4. Conclusions

After comparing and analyzing the flow field characteristics and separation performances of prismatic hydrocyclones with conventional hydrocyclones, the following conclusions can be drawn:

- (1) Prismatic hydrocyclones exhibit reduced static pressure and pressure drop compared to conventional hydrocyclones, with the most significant reduction observed in pressure drop. Additionally, the diameter of the air core in prismatic hydrocyclones decreases while the separation space increases. This indicates that prismatic hydrocyclones operate with lower energy consumption and higher processing capacity under equivalent feed conditions.
- (2) Tangential and axial velocities in prismatic hydrocyclones are lower than those in conventional hydrocyclones. The reduced tangential velocity prevents organic matter in sludge from migrating toward the wall and mixing into the outer swirling flow under high-speed centrifugal force. Lower axial velocity near the wall extends the residence time of outer swirling flow inside the hydrocyclone, facilitating more thorough particle separation and enhancing separation accuracy.
- (3) The presence of edges in prismatic hydrocyclones increases local turbulent kinetic energy near the wall, enhancing particle looseness. This promotes elutriation of organic matter adhering to grit, allowing it to re-enter the separation zone and thereby improving grit removal efficiency in sludge.
- (4) Prismatic hydrocyclones exhibit significantly lower organic matter content in the conical section compared to conventional hydrocyclones, concentrating organic matter in the hydrocyclone column segment. This concentration improves the recovery rate of organic matter in sludge, with the six-prism hydrocyclone demonstrating the best separation performance among tested configurations.

Acknowledgments

This study was financially supported by Key R&D Program of Shandong Province, China (2024TSGC0658) and Science and technology smes innovation ability improvement project of Tai'an City, Shandong Province, China(2024TATSGC006)

References

- ABDOLLAHZADEH, L., MAZRAENO, M.S., HOSSEINI, S.N., FAZLALI, A., KHATAMI, M., 2022. *Application of a 3D printed miniaturized hydrocyclone in biopharmaceutical industry-numerical and experimental studies of yeast separation from fermentation culture media*. Prep. Biochem. Biotech. 53.1, 31–39.
- ALMILLY, R.F., CHASIB, M.I., 2023. *Application of hydrocyclone in chemical precipitation*. Sep. Sci. Technol. 58.5, 995-1003.
- ANJOS, R.P.D., MEDRONHO, R.D.A., KLEIN, T.S., 2021. *Assessment of turbulence models for single phase CFD computations of a liquid-liquid hydrocyclone using OpenFOAM*. J. Turbul.22.2, 79-113.
- Bai, C.Z., Park, H., Wang, L.G., 2021. *Modelling solid-liquid separation and particle size classification in decanter centrifuges*. Sep. Purif. 263, 118408.
- CAO, Y.S., ZHENG, X.C., LIU, Z.X., VAN LOOSDRECHT, M.C.M., DAIGGER, C., 2021. *Bottlenecks and Causes, and Potential Solutions for Municipal Sewage Treatment in China*. B. J. Univ. of Technol. 47.11, 1292-1302.
- GONG, H.F., LIANG, X.X., HUO, C., PENG, Y., YIN, H., YU, B., PAN, Y., LIU, Y.Q., 2023. *Analysis of characteristics of electric field-enhanced multi-gradient of solid particles in oil*. Chem. Eng. Res. Des. 200, 374-387.
- HAMZA, J.E., AL-KAYIEM, H.H., LEMMA, T.A., 2020. *Experimental investigation of the separation performance of oil/water mixture by compact conical axial hydrocyclone*. Therm. Sci. Eng. Prog. 17, 100358.
- HOU, D.X., LIU, P.K., ZHAO, Q., JIANG, L.Y., CUI, B.Y., WEI, D.Z., 2023. *Effect of separation space on the separation performance of cylindrical hydrocyclones*. Powder. Technol. 427, 118743.
- HSIEH K.T., RAJAMANI K., 1988. *Phenomenological model of the hydrocyclone: Model development and verification for single-phase flow*. Int. J. Miner. Process. 22, 223-237.
- HSU, C.Y., WU, R.M., 2010. *Effect of Overflow Depth of a Hydrocyclone on Particle Separation*. Drying. Technol. 28.7, 916-921.
- IZQUIERDO, J., SUKUNZA, X., ESPINAZO, P., VICENTE, J., 2024. *Roberto Aguado, Martin Olazar, Quantitative assessment of the prominence of fish hooks in hydrocyclones over different operation and geometrical parameters*. Powder. Technol. 431, 119079.

- IZQUIERDO, J., SUKUNZA, X., ESPINAZO, P., VICENTE, J., AGUADO, R., OLAZAR, M., 2023. *In depth characterisation of hydrocyclones: Ascertaining the effect of geometry and operating conditions on their performance*. Adv. Powder. Technol. 34.6, 104025.
- JI, L., PAUL, P., SHANBHAG, B.K., DIXON, I., KUANG, S.B., HE, L.Z., 2023. *Emerging application of hydrocyclone in biotechnology and food processing*. Sep. Purif. 309, 122992.
- JIANG, L.Y., LIU, P.K., ZHANG, Y.K., YANG, X.H., LI, X.Y., ZHANG, Y.L., WANG, H., 2021. *The Performance Prediction Model of W-Shaped Hydrocyclone Based on Experimental Research*. Minerals. 11.2, 118-118.
- KHATRI, N., KHATRI, K.K., SHARMA, A., 2020. *Enhanced Energy Saving in Wastewater Treatment Plant Using Dissolved Oxygen Control and Hydrocyclone*. Environ. Technol. Inno. 18, 100678.
- LAVRINENKO, A.A., SYSA, P.A., 2023. *Prediction of Magnetic Hydrocyclonage Performance in Suspensions*. J. Min. Sci. 59.4, 649-657.
- LI, F., LIU, P.K., YANG, X.H., ZHANG, Y.K., LI, X.Y., JIANG, L.Y., WANG, H., FU, W.X., 2021. *Purification of granular sediments from wastewater using a novel hydrocyclone*. Powder. Technol. 393, 751-763.
- LI, F., LIU, P.K., YANG, X.H., ZHANG, Y.K., LI, X.Y., JIANG, L.Y., WANG, H., FU, W.X., 2021. *Numerical analysis on the effect of the length of arc-shaped vortex finder on the hydrocyclone's flow field and separation performance*. Miner. Eng. 172, 107172.
- LIANG, Z.T., LI, F., WANG, Y.C., HAN, H., JI, X.F., 2024. *Effects of composite structures on internal flow field and particle classification performance of hydrocyclone*. Int. J. Coal. Prep. Util. 1-22.
- LIU, Y., ZHANG, Y.B., YAN, L.H., YUAN, P., JI, L., CHU, K.W., LI, Z.Y., KUANG, S.B., 2023. *Mini-hydrocyclone performance enhancement in removing small-size microplastics using flocculants*. J. Water. Process. Eng. 53, 103755.
- NI, L., TIAN, J.Y., SONG, T., JONG, Y.S., ZHAO, J.N., 2019. *Optimizing Geometric Parameters in Hydrocyclones for Enhanced Separations: A Review and Perspective*. Sep. Purif. Rev. 48.1, 30-51.
- NOROOZI, S., HASHEMABADI, S.H., 2011. *CFD analysis of inlet chamber body profile effects on de-oiling hydrocyclone efficiency*. Chem. Eng. Res. Des. 89.7, 968-977.
- PENG, Y., ZHANG, H.H., YU, B., HUO, C., YIN, H., GONG, H.F., 2024. *Effect of electric field on separation characteristics of oil-water-solid three phases separating device*. Process. Saf. and Environ. 183, 138-151.
- RAZMI, H., GOHARRIZI, A.S., MOHEBBI, A., 2019. *CFD simulation of an industrial hydrocyclone based on multiphase particle in cell (MPPIC) method*. Sep. Purif. 209, 851-862.
- SALMANIZADE, F., MOGHADDAM, A.G., MOHEBBI, A., 2021. *Improvement hydrocyclone separation of biodiesel impurities prepared from waste cooking oil using CFD simulation*. Sep. Sci. Technol. 56.6, 1152-1167.
- SHOLL, D.S., LIVELY, R.P., 2016. *Seven chemical separations to change the world*. Nature. 532.7600, 435-7.
- SILVA, J.T.T., BICALHO, I.C., RIBEIRO, G.P., ATAÍDE, C.H., 2020. *Hydrocyclone applied in the physical processing of phosphate concentrate containing rare earth elements*. Miner. Eng. 155, 106402.
- THIEMSAKUL, D., PIEMJAIWANG, R., SEMA, T., FENG, Y.Q., PIUMSOMBOON, P., CHALERMSINSUWAN, B., 2024. *Effect of hydrocyclone design in microplastics-water separation by using computational fluid dynamics simulations*. Results. Eng. 22, 102034.
- VEGA-GARCIA, D., CILLIERS, J.J., BRITO-PARADA, P.R., 2020. *CFD modelling of particle classification in mini-hydrocyclones*. Sep. Purif. 251, 117253.
- WANG, N., LU, H., LIU, B., XIONG, T., LI, J.P., WANG, H.L., YANG, Q., 2024. *Enhancement of heavy metals desorption from the soil by eddy deep leaching in hydrocyclone*. J. Environ. Sci. 135, 242-251.
- YE, J.X., XU, Y.X., SONG, X.F., YU, J.G., 2019. *Numerical modelling and multi-objective optimization of the novel hydrocyclone for ultra-fine particles classification*. Chem. Eng. Sci. 207, 1072-1084.
- ZHANG, C.E., WEI, D.Z., CUI, B.Y., LI, T.S., LUO, N., 2017. *Effects of curvature radius on separation behaviors of the hydrocyclone with a tangent-circle inlet*. Powder. Technol. 305, 156-165.
- ZHANG, Y.K., GE, J.B., JIANG, L.Y., WANG, H., YANG, J.R., CHEN, B., 2021. *Influence of Vortex Finder Structure on Separation Performance of Double-Overflow Three-Product Hydrocyclones*. Separations. 8.6, 79.
- ZHAO, Q., HOU, D.X., CUI, B.Y., WEI, D.Z., SONG, T., FENG, Y.Q., 2021. *Development of an integrated multichannel inlet for improved particle classification in hydrocyclones*. Adv. Powder. Technol. 32.12, 4546-4561.
- ZHOU, M., FARKAS, L.A., KÖKKİLİÇ, O., LANGLOIS, R., ROWSON, N.A., WATERS, K.E., 2023. *An investigation into processing fine magnetite using a magnetic hydrocyclone*. Can. Metall. Q. 62.3, 497-501.